Tensile Deformation and Failure of Thin Films of Aging Laponite Suspension†

Asima Shaukat, Yogesh M. Joshi,* and Ashutosh Sharma*

Department of Chemical Engineering, Indian Institute of Technology Kanpur, Kanpur 208016 India

In this paper, we study deformation, failure, and breakage of visco-elastic thin films of aging laponite suspension under a tensile deformation field. Aqueous suspension of laponite is known to undergo waiting time dependent evolution of its microstructure, also known as aging, which is accompanied by an increase in the elastic modulus and relaxation time. In the velocity controlled tensile deformation experiments, we observed that the dependence of force and dissipated energy on velocity and initial thickness of the film is intermediate to a Newtonian fluid and a yield stress fluid. For a fixed waiting time, strain at break and dissipated energy increased with velocity but decreased with initial thickness. With an increase in age, the strain at break and dissipated energy showed a decrease suggesting enhanced brittle behavior with an increase in waiting time, which may be caused by restricted relaxation modes due to aging. In a force controlled mode, decrease in strain at failure at higher age also suggested enhanced brittleness with an increase in waiting time. Remarkably, the constant force tensile deformation data up to the point of failure showed experimental time−aging time superposition that gave an independent estimation of relaxation time and elastic modulus dependence on age.

I. Introduction

Understanding deformation behavior of thin films under tensile deformation field is important for many applications such as pressure sensitive adhesives,[1] bioadhesives,[2] lubricant films,[3] hip joints,[4] cosmetic and pharmaceutical creams,[5] corneal tear film,[6] etc. The materials that constitute such films are often visco-elastic soft materials with complex microstructure caused by physical or chemical cross-linking and/or by the presence of metastable phases. The high viscosity and elasticity of these materials impose significant constraints on the translational mobility of the primary structural entity that comprises the soft materials, forcing it to explore only a part of the phase space available to it.[7,8] Rheological study of such systems is always challenging, since such materials often show yield stress and thixotropic characteristics.[9] In addition, the broken ergodicity of these materials imparts aging which leads to strong history dependence. In this paper, we study the force response and dissipated energy in the tensile deformation leading to failure and breakage of thin films of aqueous suspensions of laponite. A laponite suspension is a model thixotropic visco-elastic material showing strong aging behavior, which allows us to also investigate the influence of material visco-elasticity on its tensile deformation field. The behavior of such materials under tensile loading has not been investigated previously.

The class of soft materials that show ergodicity breaking due to jamming of the primary entity are represented as soft glassy materials.[10] Although the thermal motion is not adequate to attain equilibrium, the jammed entities undergo microscopic dynamics of structural rearrangement in their arrested state and explore those configurations that take them to a lower energy state.[10,11] This phenomenon is commonly known as aging and is accompanied by significant increase in viscosity and elasticity of the material as a function of time. Prominent characteristic features common in these materials are extremely slow relaxation dynamics with dominant mode growing with the age of the system.[12] Application of the sufficiently strong deformation field imparts diffusion of the arrested entities out of their cages causing local yielding events which leads to decrease in relaxation time and its dependence on age.[10] This phenomenon is commonly known as rejuvenation. Therefore, aging and rejuvenation affect the visco-elasticity of these materials, which makes these materials demonstrate complex rheological behavior. The aqueous suspension of smectite clay laponite is considered as a model soft glassy material that shows all of the above-mentioned characteristic features[8] and, hence, is a subject of intense investigation over the past decade. Various prominent studies on this system involve optical characterization to explore its relaxation dynamics[13−20] and phase behavior[15,21−24] while various rheological tools, which essentially investigate shear flow behavior, have been employed to study aging under deformation field and thixotropic behavior.[25−30]

In many applications, thin viscous and visco-elastic layers undergo tensile deformation. Thus, deformation behavior of simple liquids such as silicon oil, oil paints, glycerol, castor oil, olive oil, etc. in a Hele−Shaw cell or in similar geometries under tension has been studied.[31−34] Finger formation during the cohesive or adhesive failure of cross-linked visco-elastic liquid and solid polydimethylsiloxane (PDMS) has also been extensively investigated.[35−43] The principle focus of such studies is to study either the variation of force required or strain induced under a variety of loading conditions or the morphology of the fingering patterns observed during the adhesive or cohesive failure. If the bonding between the plates and the fluid layer is weak, contact breaks at the boundary leading to debonding or adhesive failure.[35,44−48] On the other hand, cohesive failure occurs if the contact area of the fluid that holds two plates together decreases causing failure in the bulk of the material.[32−35,44−48] For the liquid-like films, at the higher time scales of plate separation, pressure gradients drive air into the fluid causing fingering patterns due to Saffman−Taylor instability.[32−35,48,49] For elastic solid-like films, adhesion failure also occurs by fingering, but their spacing is governed by the minimization of the stored elastic strain energy.[35−42] Thus, most of the studies concern rheologically simpler systems such as Newtonian,[32−35,44,48,50,51] linear viscoelastic,[34,35,44−47] and yield stress fluids[48,49] and their corresponding fingering instability patterns under velocity and force controlled deformation fields. In Newtonian fluids, the relationship between pulling force F

† Dedicated to Prof. Jyeshtharaj B. Joshi on the occasion of his 60th birthday.

* To whom correspondence should be addressed. E-mail: joshi@iitk.ac.in (Y.M.J.); ashutos@iitk.ac.in (A.S.).

10.1021/ie9006326 CCC: $40.75
Published on Web 07/14/2009

and constant velocity V can be obtained by solving Navier−Stokes equations under tensile deformation and is given by[48,51]

$$F = 3\pi\mu R_i^4 d_i^2 V/2d^5 \quad (1)$$

where R_i and d_i are the initial radius and thickness of the sample, respectively, μ is viscosity, and d is the distance between two plates. Derks et al.[48] extended the analysis to yield stress fluid described by the Herschel−Bulkley model in the limit of small deformation rates and obtained an expression for pulling force given by

$$F = 2\pi\mu R_i^3 d_i^{3/2}\sigma_y/3d^{5/2} \quad (2)$$

where σ_y is the yield stress. They observed an excellent agreement of this expression with the experimental behavior of systems having varying yield stress. Integration of above expression for force over a plate separation yields energy dissipated during tensile deformation. For a yield stress fluid, Derks et al.[48] observed it to be a linear function of yield stress while independent of the initial separation. The nanoclay suspension we study also shows yield stress. However, unlike the system used by Derks et al.,[48] this nonlinear suspension demonstrates strong time and deformation field dependent rheological behavior, including aging of its rheological properties.[26,27]

In this work, we investigate the force and energy response of aqueous visco-elastic suspension of laponite to applied tensile deformation field by varying the material visco-elasticity (aging time) and initial thickness under two distinct modes of deformation: constant rate of deformation (velocity) and constant normal force. A time−aging time superposition of the suspension data is employed to give an independent estimate of the dependence of the modulus and relaxation time on aging time. The process of suspension-film breakup is characterized by the strain and critical force required at the initiation of failure and the energy dissipated for a complete cohesive failure of the film. The effects of visco-elasticity (aging time) and strength of deformation field on the mode of material failure, such as brittle or viscous, are also addressed. Results are compared and contrasted with the model systems of the Newtonian and yield stress fluids.

II. Material and Experimental Procedure

Laponite is a synthetic hectorite clay and belongs to the structural family known as the 2:1 phyllosilicates.[52] Laponite is commonly used in the chemical and the food industry to control rheological properties of the end product. Laponite is composed of disk shaped particles with a diameter of 25 nm and a layer thickness of 1 nm.[53] The chemical formula for laponite is $Na_{+0.7}[(Si_8Mg_{5.5}Li_{0.3})O_{20}(OH)_4]_{-0.7}$. The surface of laponite has a permanent negative charge while the edge is less negative in the basic pH medium while positive in the acidic pH medium.[52] At pH 10, the negative charge on the surface leads to overall repulsion among the laponite particles,[15] although the attractive interactions between the edge and the surface can not be ruled out.[54] Soon after mixing laponite with water with concentrations above 1 vol % (~2.6 wt %), the system undergoes ergodicity breaking.[55]

The laponite RD used in this study was procured from Southern Clay Products, Inc. Laponite powder was dried for 4 h at 120 °C before mixing with ultra pure water at pH 10 under vigorous stirring. The basic environment is necessary to provide chemical stability to the suspension.[56] The pH 10 was maintained by the addition of NaOH. The suspension having

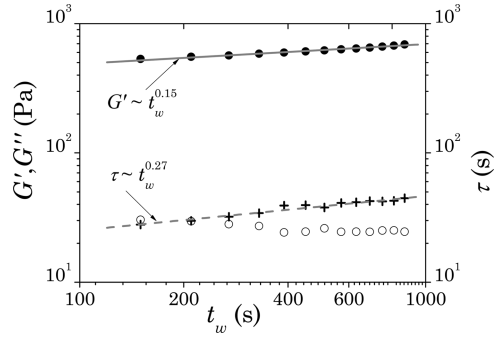

Figure 1. Evolution of elastic modulus (G', filled circles), viscous modulus (G'', open circles) and relaxation time (τ, +) as a function of waiting time ($f = 0.1$ Hz, $\gamma_0 = 1\%$). Thick gray line represents a power law fit to elastic modulus−waiting time data ($G' \sim t_w^{0.15}$), while dashed gray line represents a power law fit to relaxation time−waiting time data ($\tau \sim t_w^{0.27}$).

3.5 wt % of laponite was stirred vigorously by Ultra turrax T25 for about 1 h and left undisturbed for a period of about 3 months in a sealed polypropylene bottle. The rheological and tensile tests were carried out using the parallel plate (50 mm diameter) geometry of the Anton Paar MCR 501 rheometer. Before placing the suspension on the lower plate of the rheometer, the sample was shear melted (rejuvenated) by passing it through a syringe needle several times. Shear melting is needed to achieve a uniform initial state before beginning the experiment, and validation of the same by passing through a syringe needle was confirmed by reproducibility of the initial state. Subsequently, the upper plate was lowered until the gap between both the plates attained a predetermined value. After keeping the sample unperturbed for a desired waiting time, that was measured since a predetermined gap was set; the upper plate was pulled in a direction normal to the plates by two modes, namely a constant velocity and a constant force. In the MCR 501 rheometer, the normal force transducer has a least count of 10^{-2} N. In a force controlled mode, the normal force is controlled by the movement of the top plate. In order to avoid aging during the experiment, the experimental time was kept significantly smaller than the waiting time (age) of the sample. We have carried out the waiting time dependent experiments only up to a waiting time of 15 min, as beyond 20 min the sample started to dry at the rim of the film. In all the experiments, the temperature was maintained at 25 °C.

III. Results and Discussion

Aqueous suspension of laponite is known to undergo aging in which its elastic modulus increases with the waiting time (age).[27] Figure 1 shows an evolution of elastic and viscous modulus with waiting time in a small amplitude oscillatory experiment ($\gamma_0 = 1\%$ and frequency = 0.1 Hz). We have used the identical protocol to estimate both the moduli in an oscillatory experiment, as used in the tensile deformation experiment. It can be seen that G' increased with waiting time, and the dependence can be approximated by a power law given by, $G' \sim t_w^{0.15}$. This behavior is generally addressed as aging and is due to rearrangement of the arrested particles within the cage to attain a lower energy state.[11] If we approximate the material response as a time dependent single mode Maxwell model,[26,27] the dominating relaxation time of the material can be related to elastic and viscous modulus as: $\tau = G'/\omega G''$.[27] We have also plotted relaxation time in Figure 1, which obeyed a stronger power law dependence ($\tau \sim t_w^{0.27}$) on waiting time compared to the elastic modulus. Although the relaxation time

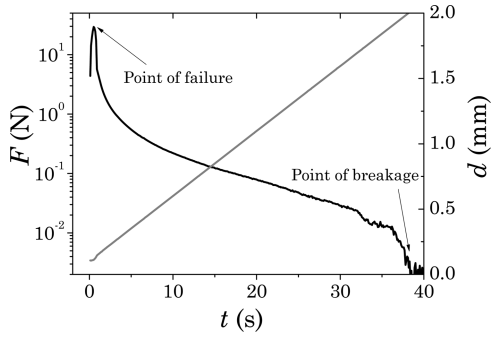

Figure 2. Variation of the normal force F (thick black line) and distance between the plates (thick gray line) as a function of experimental time t for $V = 50$ μm/s, $t_w = 15$ min, and $d_i = 107$ μm.

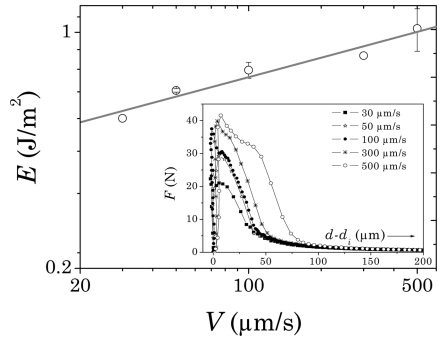

Figure 3. Dissipated energy as a function of velocity of the top plate for $t_w = 15$ min and $d_i = 105 \pm 2$ μm. The thick gray line shows a power law fit to the experimental data given by: $E \sim V^{0.2}$. (inset) Force plotted against displacement of the top plate for various velocities. The area under the curve gives energy dissipated in the tensile deformation.

is estimated by considering only a single mode of the Maxwell model, it gives a good first estimate.[27]

As mentioned before, in this work we have employed two modes: a constant velocity of the top plate and a constant pulling force to study the tensile deformation behavior. A typical response to applied constant velocity is shown in Figure 2, wherein normal force showed a rapid increase in the beginning followed by a slow decline as a function of time. The point of initiation of failure, which is represented by a maximum in the force deformation curve and the point of complete breakage are also shown in the figure. In addition, we have plotted the distance (d) between the plates as a function of time on the same figure. Except for a very short period after starting the experiment (<1 s), the rheometer maintained a constant velocity of the upper plate. It was observed that, due to separation of plates, the cross-sectional area of the suspension reduced to a fractal-like branched pattern. After the failure, the fractal pattern that connected both the plates formed fibrils and eventually underwent breakage. We discuss various characteristic features of these fractal-like branched patterns (see Figure 8) later in this section. For all the experiments carried out in this paper, the breakage occurred by cohesive failure in the bulk of the material.

The inset in Figure 3 shows variation of force as a function of movement of the top plate ($d - d_i$, where d is distance between two plates and d_i is the initial gap), for various values of velocities. These experiments were carried out on the films having thicknesses around 100 μm and at waiting time of 15 min (In the Figure 3 caption, we have mentioned initial gap to be 105 ± 2 μm. This *does not* represent the uncertainty but the range of initial gaps for the mentioned set of experiments. This is because the actual gap varies up to ± 10 μm of the gap

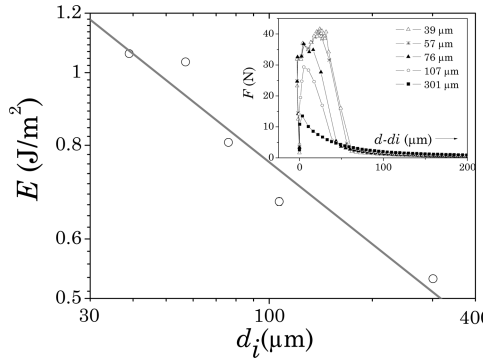

Figure 4. Dissipated energy as a function of initial gap, d_i for $t_w = 15$ min and $V = 50$ μm/s. The thick gray line shows a power law fit to the experimental data given by: $E \sim d_i^{-0.36}$. (inset) Force plotted against displacement of the top plate for various initial gaps.

prescribed in the rheometer settings). It can be seen that force at failure increased with the velocity of the top plate. We observed that the strain at break (Γ_b) also increased with increase in velocity. The area under these curves represents energy dissipated in the tensile deformation experiments. As shown in Figure 3, dissipated energy per unit initial area of the film increased with increase in the velocity of the top plate and the dependence can be represented by a power law given by $E \sim V^{0.2}$. As discussed in the Introduction, for a Newtonian fluid, dissipated energy varies linearly with velocity, while yield stress fluid with Herschel Bulkley constitutive relation shows dissipated energy to be independent of velocity. The present system showed a much weaker response compared to what is expected for a Newtonian liquid.

An initial gap between the two plates is also an important variable that affects the severity of the deformation field. We studied the effect of the same at constant velocity of top plate (50 μm/s) and constant waiting time (15 min). The corresponding energy dissipated per unit initial area, plotted in Figure 4, also showed decrease with increased initial film thickness with a power law dependence $E \sim d_i^{-0.36}$. This dependence is also significantly weaker than that for a Newtonian fluid ($E \sim d_i^{-2}$) and is closer to a yield stress fluid for which the dissipated energy is independent of the initial plate spacing. The corresponding strain at failure (Γ_f) and breakage (Γ_b) decreased with increase in the initial gap. It is apparent from the above discussion that the variation of strain at failure and break and that of dissipated energy is similar for increase in initial gap and for decrease in top plate velocity. One of the ways to assess the role of visco-elasticity is to define a Deborah number, $De = (\tau V/d_i)$, where the ratio, d_i/V represents the time scale of initial deformation and τ is the relaxation time of the suspension described in Figure 1. A large value of De (>1) denotes a dominantly elastic response, whereas $De < 1$ indicates viscous behavior. Figure 5 shows strain at break (Γ_b) and energy dissipated as a function of Deborah number. Strain at break, as well as energy dissipated, increased with Deborah number (or with decrease in time scale of deformation). It is known from the mechanical energy balance of a flowing fluid that the dissipated energy is proportional to $\sum_i \sum_j \sigma_{ij} \nabla_j u_i$,[57] where σ_{ij} is a stress tensor, ∇_j is a vector differential operator, and u_i is a velocity vector. Hence, viscous dissipation increases with a decrease in the time scale of deformation or increase in De, which is also equivalent to an increase in $\nabla_j u_i$. Therefore, these results suggest that, with increase in time scale of deformation, contribution to the dissipated energy primarily comes from viscous effects. In addition, at lower time scales of deformation, a higher strain can be supported before failure and breakage

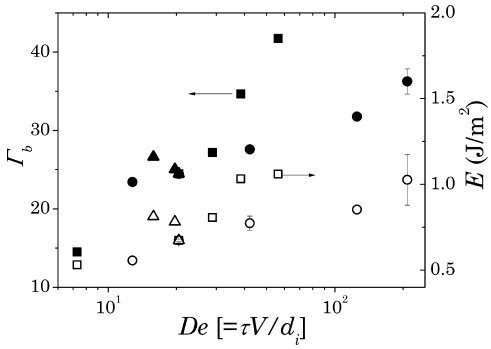

Figure 5. Strain at break (filled symbols) and energy dissipated (open symbols) in the tensile deformation leading to breakage of the film is plotted against Deborah number based on time scale of deformation for various velocity (circle), initial thickness (square), and waiting time (triangle) dependence experiments. Arrows pointing toward the left and right ordinates represent association of the open and the filled symbols with the mentioned axis.

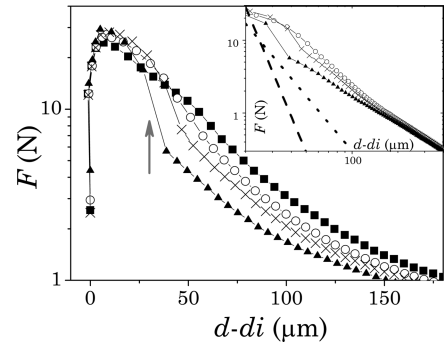

Figure 6. Force as a function of displacement of top plates for experiments carried out at various waiting times ($t_w = 0$ filled squares; 5 open circles; 10 cross; and 15 min filled triangles) for $V = 50$ μm/s and $d_i = 106 \pm 1$ μm. The gray arrow points to a sudden decrease in force over a small displacement of the top plate at higher waiting times. (inset) Same plot on a double logarithmic scale. Thick dashed and dotted lines in the inset represent a power-law prediction for a Newtonian [$F \sim (d - d_i)^{-5}$] and a yield stress fluid (Herschel−Bulkley) [$F \sim (d - d_i)^{-5/2}$], respectively.

because of the increased importance of dissipation and decreased elastic storage of the energy.

As shown in Figure 5, strain at break and dissipated energy did not depend solely on the initial time scale of deformation (d_i/V), but individually on V and d_i. We believe that three factors are responsible for such behavior. First, the energy dissipated for a viscous fluid scales as V/d_i^2.[48] On the other hand, the yield stress material is independent of initial time scale of deformation, d_i/V.[48] These trends suggest that dependence of normal force on velocity and initial thickness is different than just (d_i/V) and hence showed different responses as shown in Figure 5. The second possible reason is the continuous increase in the time scale of deformation as the experiment progresses due to increase in the distance between the plates, which causes a continuous decrease in De. Therefore, various values of initial thickness and velocity, though leading to same ratio of d_i/V may affect the tensile deformation field differently causing changes in the strain and dissipated energy. In essence, De decreases with time, whereas the values given in Figure 5 are only the initial values at the start of the experiments. The third important reason is the thixotropic character of the present system. Since the visco-elastic behavior of an aqueous suspension of laponite is highly sensitive to the deformation field,[26] partial rejuvenation of the same reduces its viscosity as the deformation progresses. This behavior, in addition to the reasons discussed above, makes the overall behavior of the suspension highly complex, and as shown in Figure 5, does not depend solely on the initial time scale of deformation, d_i/V or the initial De.

We further carried out the tensile deformation at different waiting times (ages) of the sample for constant velocity and initial suspension thickness. In Figure 1, we have observed that the elastic modulus of aqueous laponite suspension increased with waiting time (age). It is generally observed that for this class of materials, yield stress is also proportional to its elastic modulus, and thus, yield stress should also increase with time.[48] The effect of aging time (t_w) was studied for the suspension ages that are significantly larger than the time taken in the tensile test, $t_w \gg t$, so that further aging during the experiment could be neglected. Figure 5 shows that strain to break and dissipated energy both decline with De or the relaxation time, which is proportional to aging time of the suspension. The discussion below considers the effect of aging in detail.

Figure 6 shows variation of force as a function of displacement of the top plate for various ages. The inset in this figure shows a double logarithmic plot of the same data. For a Newtonian fluid and a Herschel−Bulkley model, decay in force

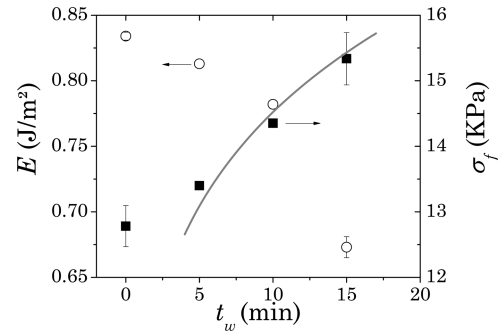

Figure 7. Energy dissipated (open circles) and stress at failure (filled squares) as a function of waiting time for $V = 50$ μm/s and $d_i = 106 \pm 1$ μm. The thick gray line represents a power-law fit to the engineering stress at failure data representing $\sigma_f \sim t_w^{0.15}$.

is expected to follow power law relations, $F \sim (d - d_i)^{-5}$ and $F \sim (d - d_i)^{-5/2}$, respectively. However, the laponite suspension showed further weaker dependence than the yield stress fluid. Engineering stress at failure and energy dissipated per unit initial area are plotted as a function of waiting time in Figure 7. It can be seen that tensile stress at failure (or force at failure) closely followed the same dependence on waiting time as that of the elastic modulus. We have neglected the point associated with the zero waiting time because aging occurred during the test and the visco-elastic properties of suspension changed over the duration of the experiment. On the other hand, unlike Herschel−Bulkley prediction,[48] wherein energy dissipated increases with the yield stress or elastic modulus, energy dissipated in the clay suspension decreased with increased waiting time and hence with increase in the elastic modulus. This result is essentially due to decrease in strain at failure and strain at break with increase in the waiting time or elastic modulus. In addition, it is apparent from the nature of the force displacement curve shown in Figure 6 that the response of material became more brittle with increase in the waiting time. It can be seen that for the force-deformation curves at higher waiting times of 10 and 15 min, the force dropped significantly after its maximum value. The severity of the drop is more for a higher waiting time sample. We have represented this by a gray arrow on Figure 6. We believe that the observed behavior is due to a corresponding increase in elastic modulus and relaxation time with waiting time. Enhancing the elastic modulus limits the dissipation while the increasingly slower relaxation process causes progressively more limited modes of energy dissipation, leading to the brittle

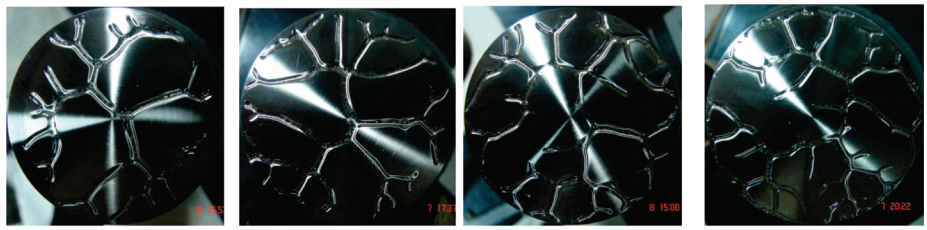

Figure 8. Photo of the upper plate after breakage. (a) $t_w = 0$ min (perimeter of the suspension−air interface per unit area = 0.2458 1/mm, number of branches = 35). (b) $t_w = 5$ min (perimeter of the suspension−air interface per unit area = 0.3215 1/mm, number of branches = 47). (c) $t_w = 10$ min (perimeter of the suspension−air interface per unit area = 0.3492 1/mm, number of branches = 54). (d) $t_w = 15$ min (perimeter of the suspension−air interface per unit area = 0.4034 1/mm, number of branches = 63). All the experiments were carried out at $d_i = 106 \pm 1$ μm and $V = 50$ μm/s.

failure in the material. We have plotted the corresponding strain to break and dissipated energy as a function of the Deborah number in Figure 5. It can be seen that the waiting time dependent data shows the opposite trend compared to the velocity and initial gap dependent data obtained at constant age. While the former experimental data showed enhanced brittle failure due to increased elasticity, the latter data showed pronounced viscous dissipation with increase in velocity and/or decrease in the initial thickness. This observation further strengthens our claim that, due to various reasons discussed above, the tensile deformation of the thin films of the aging suspension leading to its breakage does not solely depend on the Deborah number and is independently influenced by the relaxation time, elasticity, velocity, and initial thickness of the sample.

In the tensile deformation experiments on visco-elastic materials, failure occurs by fingering or fractal patterns.[32,34,35,47,58,59] We also observed identical fractal or branched patterns on both the plates upon complete separation of the plates. Figure 8 shows photographs of the top plate immediately after the complete cohesive failure in the waiting time dependent experiments. It can be seen that the contact lines, where the breakage occurred, became more branched with increase in the waiting time. We have also listed the perimeter of the suspension−air interface per unit plate area as well as number of branches of the same. It can be seen that both the properties that characterize the intensity of the branched structure increased with the waiting time. We also observed a similar enhancement in branching with an increase in the top plate velocity and with decrease in the initial gap. The effect of initial gap and top plate velocity on branching of the contact line is in accordance with Derks et al.'s[48] observations ascribed to the Saffman−Taylor instability.[49] Derks et al.[48] observed that the intensity of fingers does not have any direct correlation with dissipated energy. Interestingly, we observed that for various experiments performed at constant waiting time by varying velocity and initial thickness, increase in the intensity of branches was accompanied by increase in dissipated energy. On the other hand, for the experiments carried out as a function of waiting time, with fixed velocity and initial suspension thickness, increase in the intensity of branches showed decrease in the dissipated energy. Thus, there seems to be two different factors at work determining the branching propensity. This observation is in accordance with different trends in strain at break and dissipated energy as a function of Deborah number. Increasing the suspension elasticity or the speed of crack or finger propagation induces more frequently bifurcating and shorter cracks. The effect of higher failure speed on denser finger patterns is also seen in simple liquids.[31,33,35,48,59]

We next discuss tensile deformation of the aging suspension of laponite under constant force. Figure 9 shows a typical variation of distance between the plates under application of

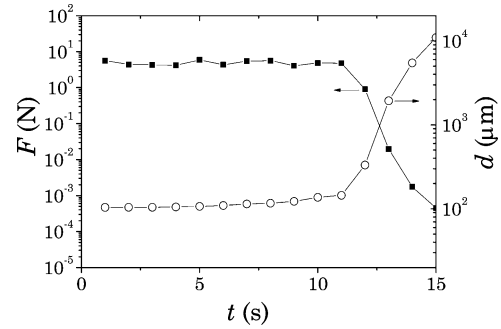

Figure 9. Pulling force measured at the top plate ($F = 5$ N) and resultant variation of the gap between the plates as a function of experimental time t for $t_w = 15$ min, $d_i = 100$ μm. Filled squares represent force while open circles represent gap.

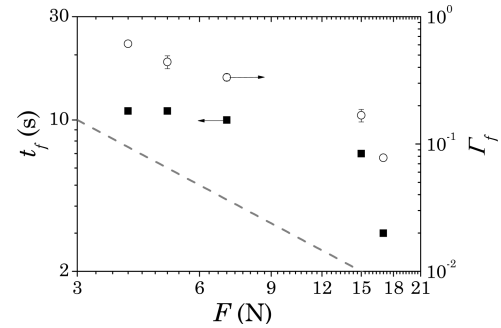

Figure 10. Time to failure (filled squares) and strain at failure (open circles) as a function of force applied to the top plate for $t_w = 15$ min, $d_i = 103 \pm 2$ μm. The thick gray dashed line represents prediction for a Newtonian fluid given by $t_f \sim F^{-1}$.

constant force. In the MCR 501 rheometer, stress is maintained by controlling the velocity of the top plate. As shown in the figure, material starts to fail at a certain critical strain and the rheometer cannot maintain a constant force thereafter. The time to failure and strain at failure mark the point at which the force starts decreasing. It can be seen from Figures 10 and 11 that both the time to failure and strain at failure decreased with increase in the applied force and initial thickness. For a Newtonian fluid, the relationship between the time of separation (which is approximately equal to time to failure) for the constant pulling force is given by the following:[34,50,60] $t_s = 3\pi\mu R_i^4/2Fd_i^2$. As shown in Figures 10 and 11, similar to that observed for the constant velocity experiments, the response of the laponite suspension is weaker compared to a Newtonian fluid.

Finally, we perform constant force experiments at various waiting times. Figure 12 shows time to failure and strain at failure as a function of waiting time. Interestingly, strain at failure decreases with the waiting time (we are disregarding the point associated with zero age, as $t \ll t_w$). Since force is constant,

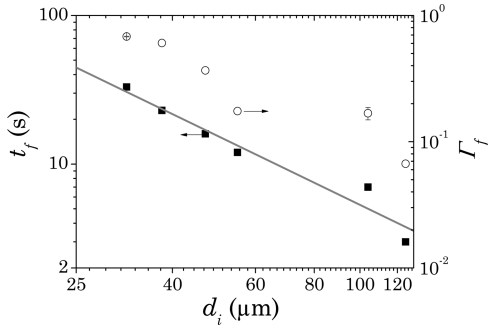

Figure 11. Time to failure (filled squares) and strain at failure (open circles) as a function of initial gap for $t_w = 15$ min and $F = 15$ N. The thick gray line shows a power law fit to time to failure data representing $t_f \sim d_i^{-1.5}$.

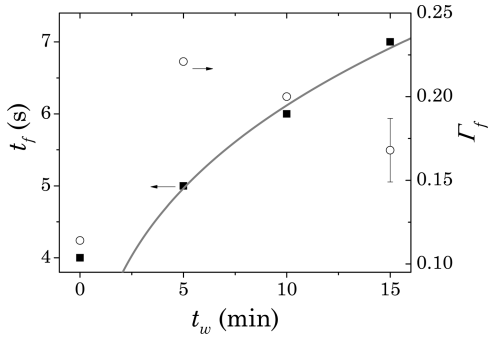

Figure 12. Time to failure (filled squares) and strain at failure (open circles) as a function of waiting time for $F = 15$ N and $d_i = 104 \pm 1$ μm. The thick gray line represents a power-law fit to time to failure dependence on waiting time given by the following: $t_f \sim t_w^{0.3}$.

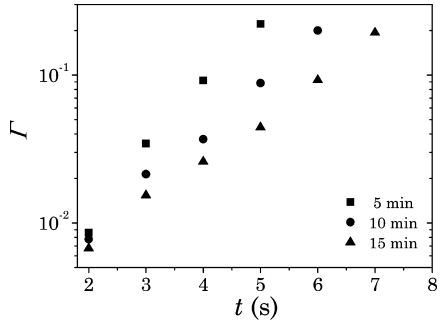

Figure 13. Tensile strain as a function of experimental time at constant force of 15 N and at different waiting times ($d_i = 104 \pm 1$ μm).

strain at failure is directly proportional to energy dissipated in causing failure in the sample, which also decreases with the waiting time. This further strengthens our observation that increase in elastic modulus induces brittleness in the system. Time to failure increases with increase in the waiting time showing a power-law dependence, $t_f \sim t_w^{0.3}$. This dependence is very close to the dependence of relaxation time on waiting time, thus suggesting a linear dependence of time to failure on relaxation time ($t_f \sim \tau$). In Figure 13, tensile strain is plotted against experimental time for three waiting times. It can be seen that the younger sample shows enhanced strain at the same experimental time (t). The dominant relaxation mode of soft glassy materials such as an aqueous suspension of laponite is known to show a power law dependence on waiting time.[12] The corresponding power law exponent, $\mu = \mathrm{d}\ln\tau/\mathrm{d}\ln t_w$, which represents the rate of increase of relaxation time, depends on the creep stress.[26,61,62] Since the relaxation processes usually intrinsically determine the rheological behavior of the material, the normalization of creep time by an appropriate characteristic

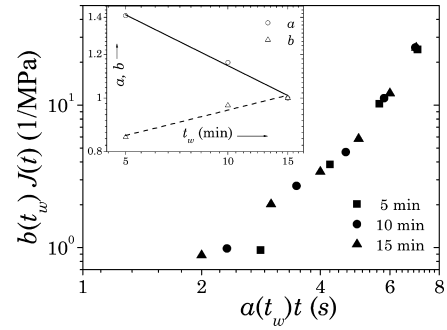

Figure 14. Superposition after carrying out horizontal and vertical shifting of experimental data shown in Figure 13. The ordinate in Figure 13 is divided by constant stress to yield compliance $J(t)$. (inset) Horizontal and vertical shift factors showing a power-law dependence on waiting time given by $a \sim t_w^{-0.31}$ and $b \sim t_w^{0.15}$, respectively.

time scale is expected to give superposition of the experimental data after appropriate vertical shifting is carried out. Figure 14 demonstrates that a horizontal and vertical shifting of tensile compliance vs time data indeed shows a successful superposition. Tensile creep compliance is obtained by dividing strain in Figure 13 by normal stress ($J(t) = \Gamma(t)/\sigma_N$). We have also plotted horizontal and vertical shift factors as a function of aging time in the inset of Figure 14. Considering a time dependent single mode Maxwell model, Joshi and Reddy[26] suggested that in order to obtain a superposition, the vertical shift factor should scale as modulus, while the horizontal shift factor should scale as inverse of relaxation time. Remarkably, horizontal shift factor ($a^{-1} \sim \tau \sim t_w^{0.31}$) and vertical shift factor ($b \sim G' \sim t_w^{0.15}$) do indeed closely match respective dependences of relaxation time and elastic modulus on age obtained from the dynamic experiments shown in Figure 1. This procedure of obtaining a universal behavior is known as creep time-aging time superposition and is generally used to obtain independent estimation of relaxation time and elastic modulus dependence on age.[63] Such a procedure is often used in polymeric glasses to predict long time tensile strain from short time tests.[63,64] Various groups have demonstrated the validity of the same concept in shear flow of soft glassy materials. However, according to best of our knowledge, this is the first report of validity of the same to the *tensile* deformation of soft glassy materials.

IV. Conclusions

In this paper, we have studied deformation, failure, and breakage of thin films of an aging suspension of laponite under a tensile deformation field. We have applied tensile deformation using two modes, namely constant velocity of the top plate and constant pulling force, as a function of initial thickness of the sample and its age. The aqueous suspension of laponite shows time dependent evolution of visco-elastic properties, also known as aging, wherein the elastic modulus and relaxation time increased with increase in the waiting time. Under the tensile deformation field, stretching of the suspension beyond a critical strain lead to the initiation of failure in the form of finger/crack/fibril formation and eventually a complete cohesive failure in the bulk of the sample with fractal-like features on the freshly formed surfaces. In a constant velocity mode, strain at failure and strain at break increased with increase in velocity, but decreased with increase in the initial thickness of the sample. In addition, the energy dissipated in the tensile deformation leading to breakage of the film increased with increase in the velocity of suspension-stretching and also with decrease in the initial suspension-film thickness. However, the dependences for

both trends were intermediate between what is expected for a Newtonian fluid and a yield stress fluid. We believe that, in the velocity and initial gap dependent experiments, increased intensity of the deformation field induces more viscous dissipation in the material. Interestingly with increase in waiting time or age, energy dissipated and strain at failure and breakage showed a decrease, demonstrating enhanced elastic or brittle response at the higher age. We believe that this behavior is caused by increase in the elasticity and relaxation time with the waiting time that restricts the modes of energy dissipation leading to rapid breakage. Overall, due to the continuously changing intensity of the flow field and thixotropy of the material, the tensile deformation behavior is observed to not be controlled by the initial Deborah number.

In a constant pulling force mode, the dependence of time to failure on the magnitude of force and initial thickness showed a weaker response than what is expected for a Newtonian fluid. For the waiting time dependent experiments, decrease in the strain at failure for older samples also indicated enhanced brittleness with age. Interestingly experimental data of tensile creep compliance normalized with the modulus at different waiting times showed a superposition when plotted against experimental time normalized with relaxation time of the system. The validation of this time−aging time superposition by tensile deformation data demonstrated the universal applicability of this procedure for soft glassy materials.

Acknowledgment

Financial support from Department of Science and Technology through the IRHPA scheme is greatly acknowledged. Y.M.J. also acknowledges partial support from the Department of Atomic Energy, BRNS young scientist award scheme.

Literature Cited

(1) Horgnies, M.; Darque-Ceretti, E.; Felder, E. Relationship between the fracture energy and the mechanical behaviour of pressure-sensitive adhesives. *Int. J. Adhes. Adhes.* **2007**, *27* (8), 661–668.

(2) Quintanar-Guerrero, D.; Villalobos-García, R.; Alvarez-Colín, E.; Cornejo-Bravo, J. M. In vitro evaluation of the bioadhesive properties of hydrophobic polybasic gels containing *N*,*N*-dimethylaminoethyl methacrylate-co-methyl methacrylate. *Biomaterials* **2001**, *22* (9), 957–961.

(3) Metzner, A. B. Extensional primary field approximations for viscoelastic media. *Rheol. Acta* **1971**, *10* (3), 434–445.

(4) Blamey, J.; Rajan, S.; Unsworth, A.; Dawber, R. Soft layered prostheses for arthritic hip joints: A study of materials degradation. *J. Biomed. Eng.* **1991**, *13* (3), 180–184.

(5) Brummer, R. *Rheology essentials of cosmetic and food emulsions*; Springer: Berlin, 2006.

(6) Sharma, A.; Ruckenstein, E. Mechanism of tear film rupture and formation of dry spots on cornea. *J. Colloid Interface Sci.* **1985**, *106* (1), 12–27.

(7) Cipelletti, L.; Ramos, L. Slow dynamics in glassy soft matter. *J. Phys. Condens. Matter.* **2005**, *17* (6), R253−R285.

(8) Bandyopadhyay, R.; Liang, D.; Harden, J. L.; Leheny, R. L. Slow dynamics, aging, and glassy rheology in soft and living matter. *Solid State Commun.* **2006**, *139* (11−12), 589–598.

(9) Barnes, H. A. Thixotropy - A review. *J. Non-Newtonian Fluid Mech.* **1997**, *70* (1−2), 1–33.

(10) Sollich, P.; Lequeux, F.; Hebraud, P.; Cates, M. E. Rheology of soft glassy materials. *Phys. Rev. Lett.* **1997**, *78* (10), 2020–2023.

(11) Wales, D. J. *Energy Landscapes*; Cambridge University Press: Cambridge, 2003.

(12) Fielding, S. M.; Sollich, P.; Cates, M. E. Aging and rheology in soft materials. *J. Rheol.* **2000**, *44* (2), 323–369.

(13) Abou, B.; Bonn, D.; Meunier, J. Aging dynamics in a colloidal glass. *Phys. Rev. E* **2001**, *64* (2 I), 215101–215106.

(14) Schosseler, F.; Kaloun, S.; Skouri, M.; Munch, J. P. Diagram of the aging dynamics in laponite suspensions at low ionic strength. *Phys. Rev. E* **2006**, *73*, 021401.

(15) Mourchid, A.; Lecolier, E.; Van Damme, H.; Levitz, P. On viscoelastic, birefringent, and swelling properties of laponite clay suspensions: Revisited phase diagram. *Langmuir* **1998**, *14* (17), 4718–4723.

(16) Bandyopadhyay, R.; Liang, D.; Yardimci, H.; Sessoms, D. A.; Borthwick, M. A.; Mochrie, S. G. J.; Harden, J. L.; Leheny, R. L. Evolution of Particle-Scale Dynamics in an Aging Clay Suspension. *Phys. Rev. Lett.* **2004**, *93* (22), 228302.

(17) Abou, B.; Gallet, F. Probing a Nonequilibrium Einstein Relation in an Aging Colloidal Glass. *Phys. Rev. Lett.* **2004**, *93* (16), 160603.

(18) Zulian, L.; Ruzicka, B.; Ruocco, G.; Capaccioli, S. Dynamics of Laponite solutions: An interpretation within the coupling model scheme. *J. Non-Cryst. Sol.* **2007**, *353* (41−43), 3885–3890.

(19) Zulian, L.; Ruzicka, B.; Ruocco, G. Influence of an adsorbing polymer on the aging dynamics of Laponite clay suspensions. *Philos. Mag.* **2008**, *88* (33−35), 4213–4221.

(20) Bhatia, S.; Barker, J.; Mourchid, A. Scattering of disklike particle suspensions: Evidence for repulsive interactions and large length scale structure from static light scattering and ultra-small-angle neutron scattering. *Langmuir* **2003**, *19* (3), 532–535.

(21) Tanaka, H.; Jabbari-Farouji, S.; Meunier, J.; Bonn, D. Kinetics of ergodic-to-nonergodic transitions in charged colloidal suspensions: Aging and gelation. *Phys. Rev. E* **2005**, *71* (2), 021402.

(22) Ruzicka, B.; Zulian, L.; Angelini, R.; Sztucki, M.; Moussaid, A.; Ruocco, G. Arrested state of clay-water suspensions: Gel or glass. *Phys. Rev. E J1−PRE* **2008**, *77* (2), 020402−4.

(23) Jabbari-Farouji, S.; Tanaka, H.; Wegdam, G. H.; Bonn, D., Multiple nonergodic disordered states in Laponite suspensions: A phase diagram. *Phys. Rev. E−Stat., Nonlin., Soft Matter Phys.* **2008**, *78*, (6).

(24) Jabbari-Farouji, S.; Wegdam, G. H.; Bonn, D., Gels and glasses in a single system: Evidence for an intricate free-energy landscape of glassy materials. *Phys. Rev. Lett.* **2007**, *99*, (6), 065701/1−065701/4.

(25) Di Leonardo, R.; Ianni, F.; Ruocco, G. Aging under shear: Structural relaxation of a non-Newtonian fluid. *Phys. Rev. E* **2005**, *71* (1), 011505.

(26) Joshi, Y. M.; Reddy, G. R. K. Aging in a colloidal glass in creep flow: Time-stress superposition. *Phys. Rev. E* **2008**, *77* (2), 021501−4.

(27) Joshi, Y. M.; Reddy, G. R. K.; Kulkarni, A. L.; Kumar, N.; Chhabra, R. P. Rheological Behavior of Aqueous Suspensions of Laponite: New Insights into the Ageing Phenomena. *Proc. R. Soc. A* **2008**, *464*, 469–489.

(28) Shukla, A.; Joshi, Y. M. Ageing under oscillatory stress: Role of energy barrier distribution in thixotropic materials. *Chem. Eng. Sci.*, published online March 26, http://dx.doi.org/10.1016.j.ces.2009.03.019.

(29) Reddy, G. R. K.; Joshi, Y. M. Aging under stress and mechanical fragility of soft solids of laponite. *J. Appl. Phys.* **2008**, *104*, 094901.

(30) Baghdadi, H. A.; Parrella, J.; Bhatia, S. R. Long-term aging effects on the rheology of neat laponite and laponite - PEO dispersions. *Rheol. Acta* **2008**, *47* (3), 349–357.

(31) Kabiraj, S. K.; Tarafdar, S. Finger velocities in the lifting Hele-Shaw cell. *Phys. A: Stat. Mech. its Appl.* **2003**, *328* (3−4), 305–314.

(32) Lindner, A.; Derks, D.; Shelley, M. J. Stretch flow of thin layers of Newtonian liquids: Fingering patterns and lifting forces. *Phys. Fluids* **2005**, *17* (7), 1–13.

(33) Poivet, S.; Nallet, F.; Gay, C.; Teisseire, J.; Fabre, P. Force response of a viscous liquid in a probe-tack geometry: Fingering versus cavitation. *Eur. Phys. J. E* **2004**, *15* (2), 97–116.

(34) Sinha, S.; Dutta, T.; Tarafdar, S. Adhesion and fingering in the lifting Hele-Shaw cell: Role of the substrate. *Eur. Phys. J. E* **2008**, *25* (3), 267–275.

(35) Nase, J.; Lindner, A.; Creton, C., Pattern formation during deformation of a confined viscoelastic layer: From a viscous liquid to a soft elastic solid. *Phys. Rev. Lett.* **2008**, *101*, (7), 074503/1−074503/4.

(36) Shenoy, V.; Sharma, A. Pattern formation in a thin solid film with interactions. *Phys. Rev. Lett.* **2001**, *86* (1), 119–122.

(37) Ghatak, A.; Chaudhury, M. K.; Shenoy, V.; Sharma, A. Meniscus instability in a thin elastic film. *Phys. Rev. Lett.* **2000**, *85* (20), 4329–4332.

(38) Reiter, G.; Sharma, A. Auto-optimization of dewetting rates by rim instabilities in slipping polymer films. *Phys. Rev. Lett.* **2001**, *87* (16), 166103/1–166103/4.

(39) Sarkar, J.; Shenoy, V.; Sharma, A. Patterns, forces, and metastable pathways in debonding of elastic films. *Phys. Rev. Lett.* **2004**, *93* (1), 018302−1.

(40) Chung, J. Y.; Kim, K. H.; Chaudhury, M. K.; Sarkar, J.; Sharma, A. Confinement-induced instability and adhesive failure between dissimilar thin elastic films. *Eur. Phys. J. E* **2006**, *20* (1), 47–53.

(41) Gonuguntla, M.; Sharma, A.; Sarkar, J.; Subramanian, S. A.; Ghosh, M.; Shenoy, V., Contact instability in adhesion and debonding of thin elastic films. *Phys. Rev. Lett.* **2006**, *97*, (1), 018303/1−018303/4.

(42) Gonuguntla, M.; Sharma, A.; Mukherjee, R.; Subramanian, S. A. Control of self-organized contact instability and patterning in soft elastic films. *Langmuir* **2006**, *22* (16), 7066–7071.

(43) Ghatak, A.; Chaudhury, M. K. Adhesion-induced instability patterns in thin confined elastic film. *Langmuir* **2003**, *19* (7), 2621–2631.

(44) Shull, K. R.; Creton, C. Deformation behavior of thin, compliant layers under tensile loading conditions. *J. Polym. Sci., Part B: Polym. Phys.* **2004**, *42* (22), 4023–4043.

(45) Creton, C.; Hooker, J.; Shull, K. R. Bulk and interfacial contributions to the debonding mechanisms of soft adhesives: Extension to large strains. *Langmuir* **2001**, *17* (16), 4948–4954.

(46) Creton, C.; Lakrout, H. Micromechanics of Flat-Probe Adhesion Tests of Soft Viscoelastic Polymer Films. *J. Polym. Sci., Part B: Polym. Phys.* **2000**, *38* (7), 965–979.

(47) Webber, R. E.; Shull, K. R.; Roos, A.; Creton, C. Effects of geometric confinement on the adhesive debonding of soft elastic solids. *Phys. Rev. E−Stat., Nonlin., Soft Matter Phys.* **2003**, *68* (2 1), 021805/1–021805/11.

(48) Derks, D.; Lindner, A.; Creton, C.; Bonn, D. Cohesive failure of thin layers of soft model adhesives under tension. *J. Appl. Phys.* **2003**, *93* (3), 1557–1566.

(49) Coussot, P. Saffman-Taylor instability in yield-stress fluids. *J. Fluid Mech.* **1999**, *380*, 363–376.

(50) McFarlane, J. S.; Tabor, D. Adhesion of Solids and the Effect of Surface Films. *Proc. R. Soc. A* **1950**, *202* (1069), 224–243.

(51) Bikerman, J. J. The fundamentals of tackiness and adhesion. *J. Colloid Sci.* **1947**, *2* (1), 163–175.

(52) Van Olphen, H. *An Introduction to Clay Colloid Chemistry*; Wiley: New York, 1977.

(53) Kroon, M.; Vos, W. L.; Wegdam, G. H. Structure and formation of a gel of colloidal disks. *Phys. Rev. E* **1998**, *57*, 1962–1970.

(54) Mongondry, P.; Tassin, J. F.; Nicolai, T. Revised state diagram of Laponite dispersions. *J. Colloid Interface Sci.* **2005**, *283* (2), 397–405.

(55) Joshi, Y. M. Model for cage formation in colloidal suspension of laponite. *J. Chem. Phys.* **2007**, *127* (8), 081102.

(56) Mourchid, A.; Levitz, P. Long-term gelation of laponite aqueous dispersions. *Phys. Rev. E* **1998**, *57* (5 suppl A), R4887−R4890.

(57) Bird, R. B.; Stewart, W. E.; Lightfoot, E. N. *Transport Phenomena*, 2nd ed.; Wiley: New York, 2002.

(58) Lemaire, E.; Levitz, P.; Daccord, G.; Van Damme, H. From viscous fingering to viscoelastic fracturing in colloidal fluids. *Phys. Rev. Lett.* **1991**, *67* (15), 2009–2012.

(59) Lindner, A.; Coussot, P.; Bonn, D. Viscous fingering in a yield stress fluid. *Phys. Rev. Lett.* **2000**, *85*, 314–317.

(60) Bhushan, B. Adhesion and stiction: Mechanisms, measurement techniques, and methods for reduction. *J. Vac. Sci. Technol. B: Microelectr. Nanometer Struct.* **2003**, *21* (6), 2262–2296.

(61) Cloitre, M.; Borrega, R.; Leibler, L. Rheological aging and rejuvenation in microgel pastes. *Phys. Rev. Lett.* **2000**, *85* (22), 4819–4822.

(62) Derec, C.; Ducouret, G.; Ajdari, A.; Lequeux, F. Aging and nonlinear rheology in suspensions of polyethylene oxide-protected silica particles. *Phys. Rev. E J1−PRE* **2003**, *67* (6), 061403.

(63) Struik, L. C. E. *Physical Aging in Amorphous Polymers and Other Materials*; Elsevier: Houston, 1978.

(64) McKenna, G. B. On the physics required for prediction of long term performance of polymers and their composites. *J. Res. NIST* **1994**, *99* (2), 169–189.

Received for review April 21, 2009
Revised manuscript received June 12, 2009
Accepted June 29, 2009

IE9006326